Structural Characterization and Drug Delivery System of Natural Growth-Modulating Peptide Against Glioblastoma Cancer

Yasemin Budama-Kilinc[1] · Serda Kecel-Gunduz[2] · Rabia Cakir-Koc[1] · Bahar Aslan[3] · Bilge Bicak[2,4] · Yagmur Kokcu[4] · Aysen E. Ozel[2] · Sevim Akyuz[5]

Abstract

The aim of the current study was to design a drug delivery nano-system of natural growth-modulating peptide known as GHK that naturally occurs in human plasma, saliva, and urine and determine possible anticancer activity against glioblastoma cancer based on *in-silico* and *in-vitro* evaluations. In this current study, a drug delivery nano-system based on Poly(ε-caprolactone) (PCL) were prepared by a double emission-precipitation method with different preparation parameters for optimization. The characterization of the optimum nanoparticles was performed with Zeta-Sizer, Ultraviolet–Visible (UV–Vis), Fourier Transform Infrared spectroscopy (FT-IR) and Raman spectroscopy, and Transmission Electron Microscopy (TEM) methods. The optimum size of the GHK loaded PCL nanoparticle was prepared with a 232.5 ± 0.72 nm average particle size, -10.8 ± 0.64 mV zeta potential, and a 0.029 polydispersity index, 82.3% of encapsulation efficiency and 73% of loaded efficiency. In vitro cytotoxicity test revealed that the GHK loaded PCL nanoparticles had anticancer effect on glioblastoma cells. In vitro release study showed the sustained release behavior of GHK from nanoparticles during the period of 10 days study. In addition, molecular dynamics and molecular docking calculations, in vitro release study, and cytotoxicity tests showed that GHK loaded PCL nanoparticles may be used effectively for glioblastoma cancer therapy.

Keywords Tripeptide · Poly(ε-caprolactone) · Nanoparticle · Molecular docking · Computational design

Introduction

Peptides are small chain of amino acids. They are used in medicinal (Karahan 2021), cosmetic and dietary products due to the their unique properties (Park et al. 2021; Türkoğlu and Erdem 2010).

Natural growth-modulating peptide (GHK) is a tripeptide discovered by Pickart et al. (Pickart et al. 1980) has

✉ Yasemin Budama-Kilinc
yaseminbudama@gmail.com

[1] Department of Bioengineering, Yildiz Technical University, Istanbul, Turkey

[2] Physics Department, Istanbul University, Istanbul, Turkey

[3] Graduate School of Natural and Applied Sciences, Yildiz Technical University, Istanbul, Turkey

[4] Graduate School of Engineering and Sciences, Istanbul University, Istanbul, Turkey

[5] Department of Physics, Istanbul Kultur University, Bakırköy, Istanbul, Turkey

many biological actions on the body. Some of the biological actions of GHK has including gastric ulcer and duodenal ulcer repair and influence the improvement of bone tissue, systemic wound healing initiation, dermal wound healing, skin remodeling, and hair follicle expansion. It also leads to an increase of anti-oxidant and anti-inflammatory activities, the root secretion of human keratinocytes, and decorin, angiogenesis, and nerve outgrowth (Choi et al. 2012; Kang et al. 2009; Pickart 2008, 2009; Pickart and Margolina 2012; Pickart et al. 2012). Age is an important factor in the achievement and capacity of these biological actions. The level of GHK in plasma is about 200 ng/mL (10^{-7} M) at age 20 but declines to 80 ng/mL by age 60. This decline in the GHK-level coincides with a noticeable decrease in the regenerative capacity of an organism (Pickart et al. 1980).

GHK has been responsible for gene expression changes for certain cancers and chronic obstructive pulmonary disease (Pickart et al. 2017). GHK effects on cancer are investigated in lots of research article. One of these studies was about the metastatic human colon cancer was investigated by Broad Institute's. In studies of metastatic human colon

cancer, the Broad Institute's Connectivity Map showed that GHK among the 1309 bioactive molecules studied reversed the expression in 70% of 54 over-expressed genes (Pickart et al. 2017). In addition, GHK has been found to reactivate apoptosis different human cancer lines in cell culture.

Cancer is the most distressing disease that enforces a severe death toll worldwide. Chemotherapy is a common option for cancer treatment, but that is often limited because of its unwanted toxic effects on normal tissues. Because most anti-cancer agents are not distributed in the target tumor-bearing tissues, which results in their reduced therapeutic efficacy (Bilensoy et al. 2009; Guo et al. 2011). Over the past three decades, polymeric nanoparticles have a preferred nanoscale drug delivery vehicle to treat cancer because of their excellent endocytosis efficiency, passive tumor-targeting ability, high encapsulation efficiency, and ability to deliver a wide range of therapeutic agents (Brannon-Peppas and Blanchette 2004; Brigger et al. 2012; Budama-Kilinc et al. 2017; Çalman et al. 2019; Peer et al. 2007). PCL has been approved by the Food and Drug Administration for various biomedical applications as a non-toxic degradation product. Although there are numerous studies on the synthesis of PCL micro/nanoparticles for drug delivery applications (Paulo et al. 2011; Shuai et al. 2004), PCL is an extremely hydrophobic polymer that cannot form nanoparticles spontaneously in the absence of any emulsifier or stabilizer (Chawla and Amiji 2002). Therefore, coating/blending with large molecules such as polysaccharides or macromolecules is necessary to prevent aggregation and provide better stabilization to nanoparticles.

The docking method is a powerful tool and essential technique to describe protein–ligand and protein–protein interactions and the behavior of nanomaterials (Yuriev et al. 2011). This method can model atomic-level interactions between ligands and receptors (protein, macromolecule, DNA, RNA, etc.), which allows us to explain the basic biochemical processes by characterizing the behavior of small molecules in the binding site of target proteins (Taylor et al. 2002). The determination of the inhibition of the VEGF signaling pathway has become an important review topic for cancer treatment in recent years (Hicklin and Ellis 2005).

The aim of this study was to develop GHK-loaded PCL nanoparticles with appropriate surface modifications and well-defined particle sizes that can improve the cell uptake of GHK. This was the first time that GHK-loaded PCL nanoparticles were prepared by the double emission precipitation method. Meanwhile, the physicochemical characteristics and in vitro anti-cancer efficiency of nanoparticles were investigated. Furthermore, the anticancer activity of GHK and GHK-loaded PCL nanoparticles were studied by cellular metabolic activity assay (XTT). Intermolecular bonds that have a great influence on activity and selectivity were investigated with the help of molecular docking calculations to

understand the most likely poses with which GHK binds to protein.

Experimental Details

Materials

PCL (Mn = 80,000) and polyvinyl alcohol (PVA) (Mw = 31.000–50.000, 87–89%) were purchased from Sigma–Aldrich (USA). GHK (Mw = 400.43) was purchased from Active Peptide Co. Ltd. (USA). Dichloromethane was also purchased from Merck Millipore (> 99.5%) (Darmstadt, Germany). All other chemicals used in this paper were analytical grade. Ultrapure water from Millipore Milli-Q Gradient System was used to prepare the solutions.

Synthesis of GHK Encapsulated PCL Nanoparticles

GHK-loaded PCL nanoparticles were synthesized by the double emulsion precipitation method (Lamprecht et al. 2000; Yang et al. 2001). Briefly, 1.5 mg of GHK was dissolved in 2 mL distilled water, 30 mg of PCL was dissolved in 2 mL dichloromethane (DCM), and the PCL solution was added to the GHK solution. They were mixed and sonicated for four minutes with an ultrasonicator (Bandelin, Sonopuls) at 55 W. After that, this solution was pulled with a syringe and then added dropwise into 4 mL of 5% PVA solution under continuous stirring. After that, the solution was sonicated again for four minutes. The mixture was left overnight under continuous stirring. Finally, the obtained GHK-loaded PCL nanoparticles were centrifuged at 10,000 rpm for 30 min (Hettich, Germany) then the supernatant was discarded; this step was repeated three times and re-suspended with 10 mL of distilled water solution for further characterization and applications. The optimum particle size and size distribution of nanoparticles was obtained by using different amounts and concentrations of PVA (1%; 2%; 3%; 4%; 5%), PCL (30; 60; 90; 120; 150 mg), and GHK (0.5; 1; 1.5; 2; 3 mg).

Average Particle Size, Polydispersity Index, Particle Size Distribution, and Zeta Potential Measurement

A Zeta-sizer Nano ZS (Malvern Instruments, UK) instrument equipped with a 4.0 mV He–Ne laser (633 nm) was used to examine the properties of the average size, polydispersity index (PdI), and size distribution of nanoparticles. Every electrophoretic light scattering measurement was performed at 25 °C and each sample was prepared with phosphate-buffered saline (PBS) before filtering with 0.2 μm regenerated cellulose membrane (Sartorius, Germany).

Transmission Electron Microscopy (TEM) Observation

The morphology of GHK-loaded PCL nanoparticles was observed via Transmission Electron Microscopy (TEM) (JEOL JEM 1400 Plus). Briefly, each sample was diluted with distilled water, and placed directly into an ultrasound bath at room temperature for two minutes, then two or three drops of the sample were deposited on a Formvar-coated carbon-supported copper grid, and TEM images were observed at 120 kV.

FT-IR and Raman Analysis

FT-IR and Raman spectral analysis were implemented to investigate the possible chemical interactions between GHK and PCL polymer. The IR analyses of the samples were carried out by using both IR transmittance and reflectance (ATR) techniques. The FT-IR spectra for GHK peptide and GHK-loaded PCL nanoparticles were obtained using a Jasco 6300 FT-IR spectrometer in the range 4000–400 cm^{-1} with 2 cm^{-1} resolution. The Jasco NRS-3100 micro-Raman spectrometer was used to record the Raman spectrum of the GHK peptide and GHK-loaded PCL nanoparticles. The Raman system, which was calibrated with a silicon semiconductor using the Raman peak at 520 cm^{-1}, has three gratings (600, 1200, and 1800 lines/mm) and two laser sources (532 nm green laser and 785 nm red laser), three Olympus microscope lenses ($20\times$, $50\times$, $100\times$), and a high-sensitivity cooled CCD detector. The GRAMS/AI 7.02 (Thermo Electron Corporation) software package was used to acquire the baseline adjustment, smoothing, second derivative and band fitting procedures. Using the Gaussian function, band fitting was performed until the reproducible and converged results were obtained from the squared correlations better than $r^2 \sim 0.9999$. The 2nd derivative function that was obtained using the Savitzky–Golay function (two polynomial degrees, five points) was used to determine the band positions and band widths for band fitting.

Encapsulation and Loading Efficiency of the Nanoparticles

First, the standard curve of GHK was obtained using a UV–Vis spectrometer (Shimadzu, Japan) at 220 nm. The encapsulation and loading efficiency of GHK-loaded PCL nanoparticles were measured by separating the nanoparticles from the aqueous nanoparticle suspension via centrifugation (Govender et al. 1999). The concentration of free GHK in the supernatant was determined by a UV–Visible Spectrometer via the GHK standard calibration curve.

The encapsulation and loading efficiency of GHK were respectively calculated by the following formulae:

$$\text{Encapsulation Efficiency} = \frac{\text{Total GHK amount} - \text{Free GHK amount}}{\text{Total GHK amount}} \times 100 \qquad (1)$$

$$\text{Loading Efficiency} = \frac{\text{Encapsulated GHK amount}}{\text{Total nanoparticles weight}} \times 10 \qquad (2)$$

In vitro Release Study

The in vitro GHK release profiles were determined from PCL nanoparticles using GHK-loaded PCL nanoparticles that were obtained from one set of preparations and re-dispersed in 10 mL of distilled water at a final concentration of 150 µg/mL. A time-dependent release study was carried out at time intervals of 0; 0.5; 1; 2; 3; 6; 7; 9; 10; 24; 72; 96; and 240 h. Samples were incubated at 37 °C under gentle agitation. At proper time intervals, the intake amounts of GHK in loaded nanoparticles were first extracted in PBS and then quantified spectrophotometrically. The concentration of GHK was determined via the GHK standard calibration curve. The release of GHK was determined as per the following equation:

$$\text{Release (\%)} = \frac{\text{Released GHK}}{\text{Total GHK}} \times 100 \qquad (3)$$

In vitro Cytotoxicity of GHK, PCL Nanoparticles, and GHK-Loaded PCL Nanoparticles

A mouse fibroblast cell line (L929) was used to determine the cytotoxicity of GHK, PCL nanoparticles, and GHK-loaded PCL nanoparticles. L929 cells were cultured in a DMEM-F12 medium (including 10% Fetal Bovine Serum and Penicillium-Streptomycin) at 37 °C (5% CO_2) and proliferated cells were trypsinized. Cells were seeded in sterile 96-well flat bottom microplates with 10^4 cells in each well. All samples were added to cultured cells at different concentrations (0–100 µg GHK in 1 mL) and incubated for 24 h at 37 °C (5% CO_2). After that, the medium was replaced with 100 µL of 2,3-Bis-(2-Methoxy-4-Nitro-5-Sulfophenyl)-2H-Tetrazolium-5-Carboxanilide (XTT) solution in DMEM (0.5 mg/mL concentration with 7.5 µg/mL Phenazine methosulfate). Plates were incubated for four hours at 37 °C and the optical density was measured at 450 nm with a multiplate reader (Thermo LabsystemsMultiskan Ascent 354 Microplate Photometer).

In vitro Anticancer Efficiency of GHK

Human U87 glioblastoma cells were used to determine the anticancer efficacy of GHK tripeptide. L929 cells were used for comparison; U87 cells were cultured in DMEM-F12 medium (including 10% Fetal Bovine Serum and Penicillium-Streptomycin) at 37 °C (5% CO_2) and proliferated cells were trypsinized. GHK was added at different concentrations (0–40 mg/mL) on both the U87 cells and L929 cells and incubated for 24 h (Kokcu et al. 2020). XTT was applied as mentioned above and the optical density was measured.

Molecular Dynamic (MD) Simulation

Molecular dynamic simulation of Gly-His-Lys tripeptide with PCL and PVA polymers was performed with GROMACS 2019.1 program (Van Der Spoel et al. 2005) using a AMBER-99SB- ILDN force field (Hornak et al. 2006) for 10 ns and TIP4P water models (Abascal and Vega 2005). For the molecular dynamic study, Gly-His-Lys was prepared with the help of Gaussian software (Frisch et al. 2009) by using the results of optimization geometry that were calculated. PCL and PVA polymers were prepared for molecular dynamic study using Gaussian software program (Frisch et al. 2016), AmberTools18 (Case et al. 2018) and ACPYPE tool (Da Silva and Vranken 2012). 1 GHK molecule, 10 PCL and 4 PVA polymers were placed in a box (10x10x10).

The steepest descent integrator was initially performed for energy-minimization. The whole system was heated until the temperature and pressure were fixed using the NVT (for 100 ps) and NPT (for 100 ps) ensemble. Temperature coupling was implemented with a V-rescale (velocity rescaling) thermostat (Bussi et al. 2007) at 310 K while pressure coupling was carried out with an isotropic Parinello–Rahman barostat (Parrinello and Rahman 1981) at 1 bar with a coupling time constant of 0.1 ps and 2.0 ps with 4.5×10^{-5} compressibility, respectively. The system configurations (atom coordinates, velocities, and energies) were saved at every step. XMGRACE (Turner 2005) and VMD (Humphrey et al. 1996) softwares were used to view the energy graphs and system box.

Molecular Docking and ADME Properties

The docking calculations were achieved using the Glide SP (standard precision) module of the Maestro version 11.4 in the docking calculations were achieved using the Glide SP (standard precision) module of the Maestro version 11.4 in the Schrodinger Software program (Schrödinger Release 2017–4: Maestro, Schrödinger, LLC, New York, NY, 2017)

(Friesner et al. 2004; Halgren et al. 2004). First, the most appropriate conformation of Gly-His-Lys (GHK) tripeptide obtained from the result of the molecular dynamic calculation was used to prepare for docking calculations by the LigPrep tool in the Maestro 11.4 version of the Schrödinger Software program using the OPLS force field (Harder et al. 2016). Thirty-two possible stereoisomers were produced for the ligand after selecting the ionization states at pH 7.0 ± 2.0. For protein preparation, the structure of Vascular Endothelial Growth Factor Receptor 2 (VEGFR2) kinase domain in a complex with a benzimidazole inhibitor (PDB code: 2QU5) (Potashman et al. 2007) was downloaded from the protein data bank. The SWISS-MODEL server was used to achieve a better protein homology model (Bienert et al. 2017). The receptor used as the target for molecular docking calculations was prepared using the Protein Preparation Wizard tool (Sastry et al. 2013). In the process of preparing the protein for docking, all water was removed, polar hydrogen was added, bond orders were assigned, charges were defined using PROPKA (Søndergaard et al. 2011) at pH 7.0, and receptor was optimized. Energy minimization was implemented by preferring 0.3 Å RMSD and the OPLS3 force field to converge heavy atoms. A receptor grid generation tool was utilized to generate a grid in which ligand protein binding poses were possible throughout the docking process in the active site. By defining routable groups of an active site, a cubic box was formed that was centered on the centroid of the ligand with specific dimensions and a ligand docking tool was employed to achieve ligand-receptor docking. Absorption, distribution, metabolism, and excretion (ADME) properties were also calculated using the Qik-Prop module of the Schrodinger software to specify the physicochemical and biological functional properties such as the molecular weight (MW), percent human oral absorption, predicted octanol/water partition coefficient (QPlogPo/w), polar surface area (PSA), and number of violations of Lipinski's rule of five (Lipinski et al. 1997), which is important for generating an effective drug in new drug development.

Statistical Analysis

Averages of the data obtained from the experimental and control groups were compared using the SPSS (version 24.0, SPSS Science, Chicago, IL) program. First, it was tested whether the obtained data showed normal distribution. Analysis of variance of the mean of the group with normal distribution was compared with a parametric test ANOVA. Homogeneous variances were compared with the Tukey HSD test. $P < 0.05$ was accepted as significant in all statistical evaluations.

Results and Discussion

Optimization studies were performed for blank PCL nanoparticles using different combinations of amounts of PVA (1%; 2%; 3%; 4%; 5%) and PCL (30; 60; 90; 120; 150 mg). The details of component amounts were given in Table S1. The optimum particle properties such as the average particle size, polydispersity index, particle size distribution, and zeta potential measurement were determined using a Zeta Sizer. The results of these experiments determined four PCL–PVA combinations: 1%–150 mg, 3%–150 mg, 4%–30 mg, and 5%–30 mg; these were determined to possibly be optimum blank PCL nanoparticles. Finally, these four combinations were used to assess the GHK-loaded nanoparticles using different amounts of GHK (0.5, 1, 1.5, 2, and 3 mg). All Zeta-Sizer results of nanoparticle optimization experiments were given in Table S2. Consequently, the component ratios of the optimum blank PCL were determined as 150 mg PCL for 1% or 3% PVA and 30 mg PCL for 4% or 5% PVA. Experiments were continued to prepare the GHK-loaded PCL optimum nanoparticles using five different amounts of GHK (0.5, 1, 1.5, 2, and 3 mg). In the direction of data obtained from

optimization experiments, further studies were continued by selecting the 30 mg PCL–5% PVA–1.5 mg GHK combination as the optimum nanoparticle.

Figure 1a-b give the results of the Zeta-Sizer analysis of blank PCL nanoparticles. According to the results, in the particle size distribution by volume graphic, as seen in Fig. 1a, PCL nanoparticles had a narrow size distribution with 0.035 polydispersity index and 224.4 ± 3.87 nm average particle size. In the zeta potential graph of PCL nanoparticles as seen in Fig. 1b, the zeta potential value of PCL nanoparticles was obtained as -9.79 ± 0.56 mV. Shown in the Fig. 1c, the GHK-loaded PCL nanoparticles also have a narrow size distribution with 0.029 polydispersity index and 232.5 ± 0.72 nm average particle size. In the Zeta potential graph of GHK-loaded PCL nanoparticles as seen from (Fig. 1d), GHK-loaded PCL nanoparticles were obtained with -10.8 ± 0.64 mV zeta potential value.

When compared our results with the literature values, it was observed that the average particle size, PdI and zeta potential values we obtained were appropriate (Kumar 2019; Öztürk et al. 2017; Tinca et al. 2020). For example, in the PCL nanoparticle studies conducted by Tinca et al., it was reported that the average particle size values varied
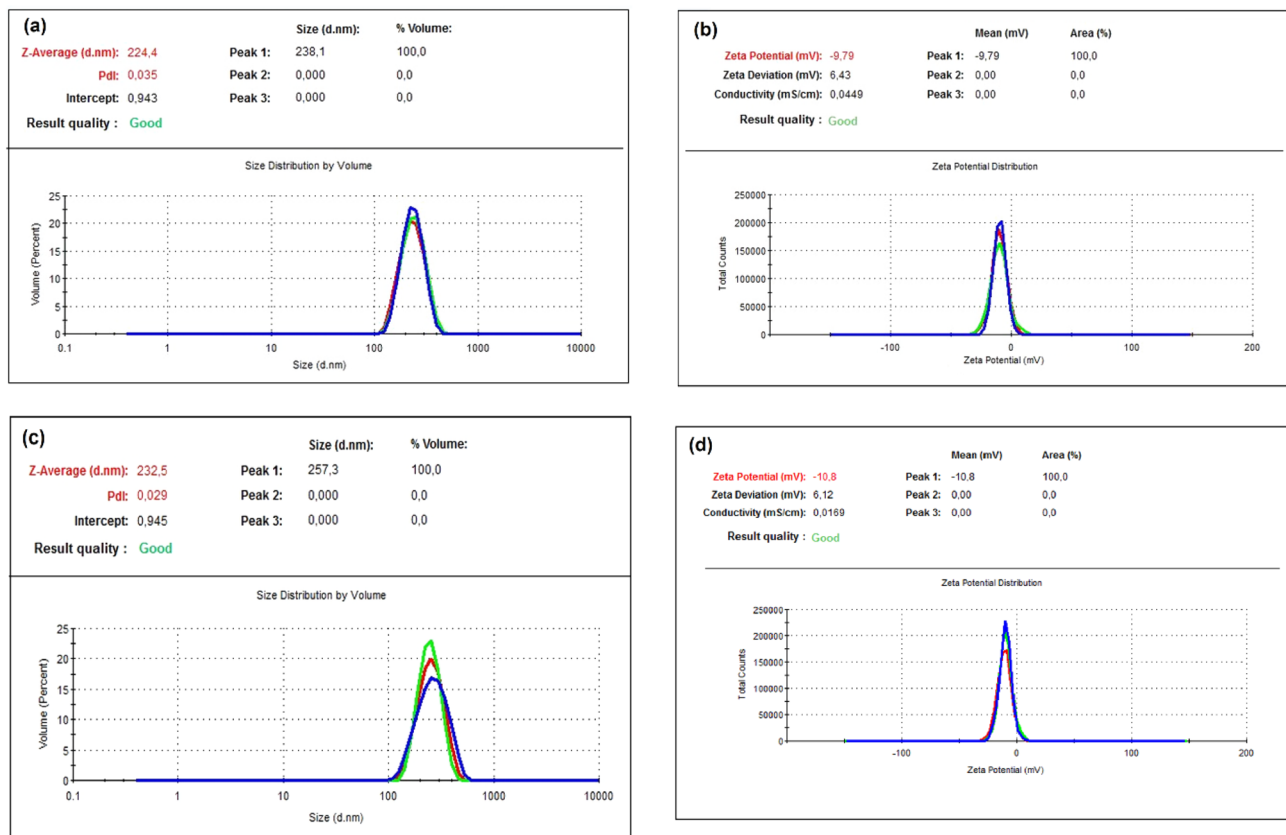

Fig. 1 Size distribution (**a**) and zeta potential (**b**) graphics of the PCL nanoparticles. Size distribution (**c**) and zeta potential (**d**) graphics of the GHK loaded PCL nanoparticle

from 210.4 ± 2.3 nm to 353.7 ± 5.6 nm, and the zeta potential varied from -6.3 ± 0.2 mV to -33.6 ± 0.5 mV. In addition, it was reported that PdI values varied from 0.033 ± 0.023 to 0.134 ± 0.026 in the same study (Tinca et al. 2020). In noscapine loaded PCL study, size range was determined from 150 to 818 nm and zeta potential range was determined from -8.8 to -16.6 mV (Kumar 2019). When we compare the blank nanoparticles with a study conducted in 2018 (Abamor 2018), the size determined as 220 nm in the literature was determined at 224 nm, which is a value very close to the value in the literature in our study. When we compare the PdI values and the zeta potential value with same literature, it was determined that our PdI values are quite low, and the zeta potential is higher compared to the literature. In the study conducted by Kolluru et al., The sizes of the blank PCL nanoparticles were lower than the value we obtained, but the PdI and zeta potential values are high. When looking at the loaded PCL nanoparticles, it was seen that our nanoparticle size is larger and the PdI and zeta potential values are lower (Kolluru et al. 2020).

Loading and Encapsulation Efficiency of GHK

As shown in Fig. 2a, the standard curve of the GHK was prepared by UV–Vis analysis at 220 nm to calculate the encapsulation efficiency of the GHK-loaded PCL nanoparticles. The encapsulation efficiency of GHK was calculated via Eq. 1 as 82.3%. This indicated that the GHK-loaded PCL nanoparticles were obtained successfully. In a study conducted with PCL nanoparticles, it was found that the encapsulation efficiencies ranged from 38 to 79%. It was determined that the percentage value we obtained in our study was higher than that obtained in the literature (Kumar 2019). In the another study, encapsulation effectiveness was determined as 64% (Abamor 2018). The

amount of GHK in the total GHK-loaded PCL nanoparticle mass was calculated via Eq. 2. The loading efficiency of the GHK-loaded PCL nanoparticles was determined as 0.73%. When compared with the study conducted by Kolluru et al., it was observed that the encapsulation efficiency was compatible with the literature and the loading efficiency was slightly lower (Kolluru et al. 2020).

In vitro Release Profile of GHK

In vitro release profile of the GHK was determined by placing 1 mL of GHK-loaded PCL nanoparticles in dialysis capsules. The dialysis capsules were placed in 250 mL of pH 7.4 PBS and UV–Vis measurements were taken at 220 nm. The process was continued for 240 h, and it was calculated via Eq. 3. It was found that 78.86% of the GHK was delivered in of the process Fig. 2b. In the literature, PCL nanoparticles released about 58% quercetin at the end of 240 h (Abamor 2018). In this study, it was seen that the release percentage is higher in the same period. In the another literature, it was stated that the drug release occurs at a rate of approximately 28% at the end of 24 h. However, in this study, it was observed that the amount of drug released in 24 h was less than 10% (Lokhande et al. 2015).

TEM Results

The morphology of the GHK-loaded PCL nanoparticles was determined by TEM. According to the TEM images, the GHK-loaded PCL nanoparticles showed distinct spherical particles with a solid dense structure. As shown in Fig. 3, the TEM images indicated that the GHK-loaded PCL nanoparticles showed a uniform size distribution with mean size 100 ± 20 nm.
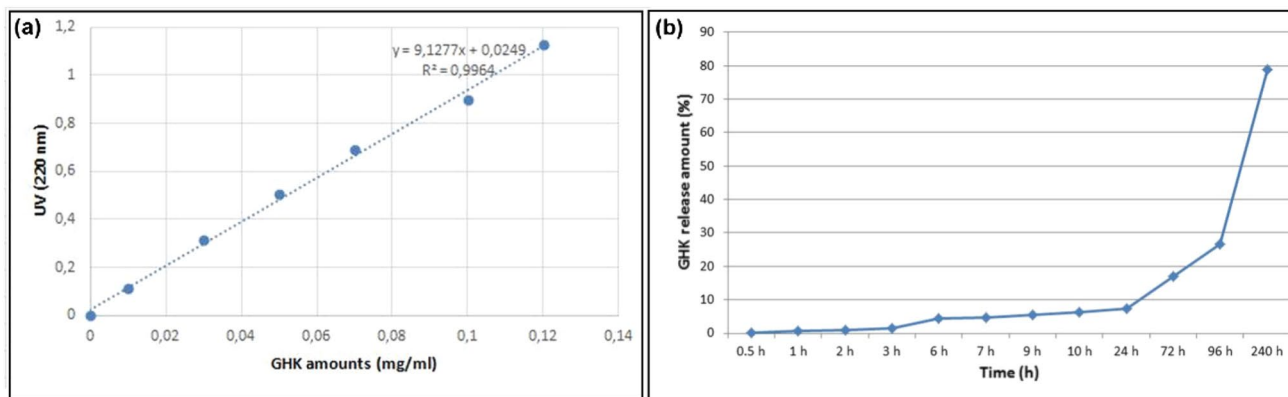

Fig. 2 The standard curve of the GHK (**a**), the in vitro release graphic of the GHK (**b**)
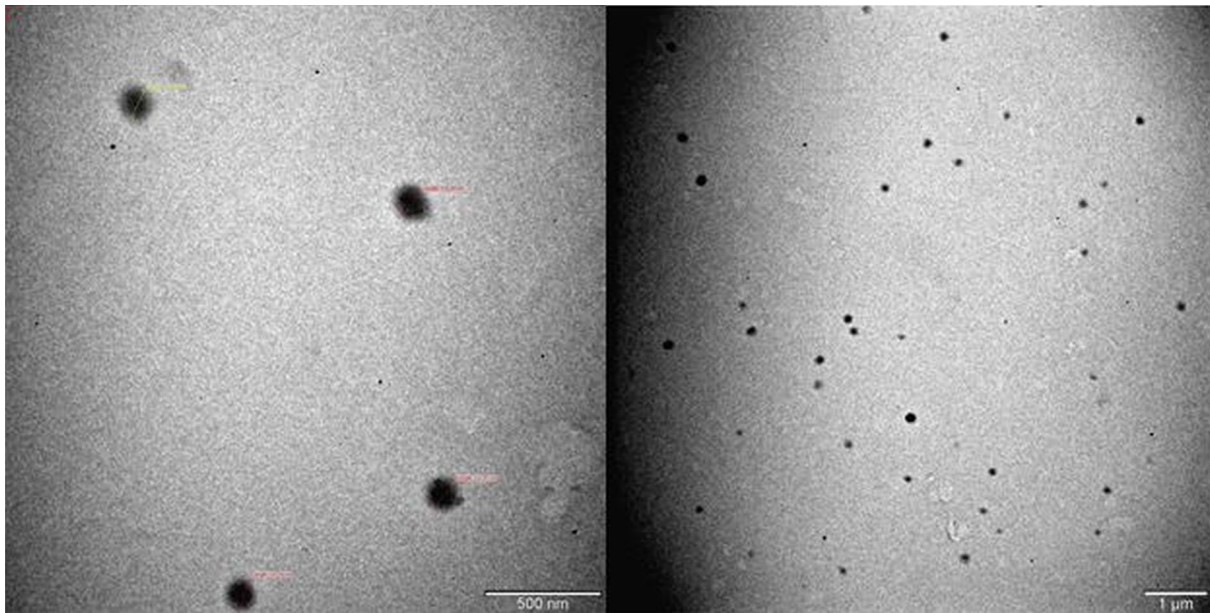
Fig. 3 Transmission Electron Microscope image of the GHK loaded nanoparticles
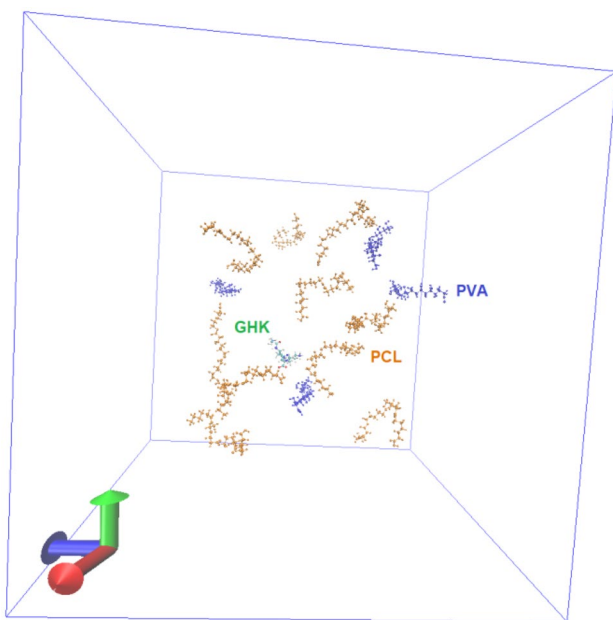

Fig. 4 The cubic box including GHK tripeptide, PCL and PVA polymers

In another study, peptide loaded PLGA nanoparticles were investigated and the particle size was measured as 139.01 nm (Kokcu et al. 2020).

MD Results

The system was generated using ideal geometries of GHK and polymers into a cubic box (see Fig. 4) with water molecules of the TIP4P water model. After the 1820-step energy minimization with the steepest-descent algorithm, potential energy converged to a large negative number, -1.7269×10^6 kj/mol in Fig. S1. The temperature (310 K) and pressure (1 bar) were stabilized with the NVT and NPT ensembles, respectively. Finally, MD simulation was performed to equilibrate the system for a 10 ns total of 5,000,000 steps with 2 fs time step. Average potential, kinetic and total energies of system were obtained and shown in Fig. S2. The Root Mean Square Deviations (RMSD) value of GHK in the system was calculated after the MD simulation. RMSD shows how much the structure has changed over the course of the simulation. Changes < 2 Å are acceptable, which mean that the peptide does not tend to deviate from its first form. The backbone RMSD graph for GHK in the system demonstrated that the peptide remained very stable and do not exceed 0.11 nm (see Fig. S3). Kokcu et al. showed that GHK has stable form in water and methanol environments by looking at RMSD changes (Kokcu et al. 2020). Compared with literature, in this study, it was observed that GHK in the system including water and polymer molecules stay in stable form by looking at RMSD changes. MD study of GHK tripeptide with the polymers used in the nanoparticle study was first in the literature.

Molecular Docking Results

The energy of the docking score obtained for GHK in the active side of the protein was -6.372 kcal/mol, as shown in Table S3 and Fig. 5a and Fig. S4. The binding pocket of the VEGFR2 protein for GHK contains a hydrophobic region as
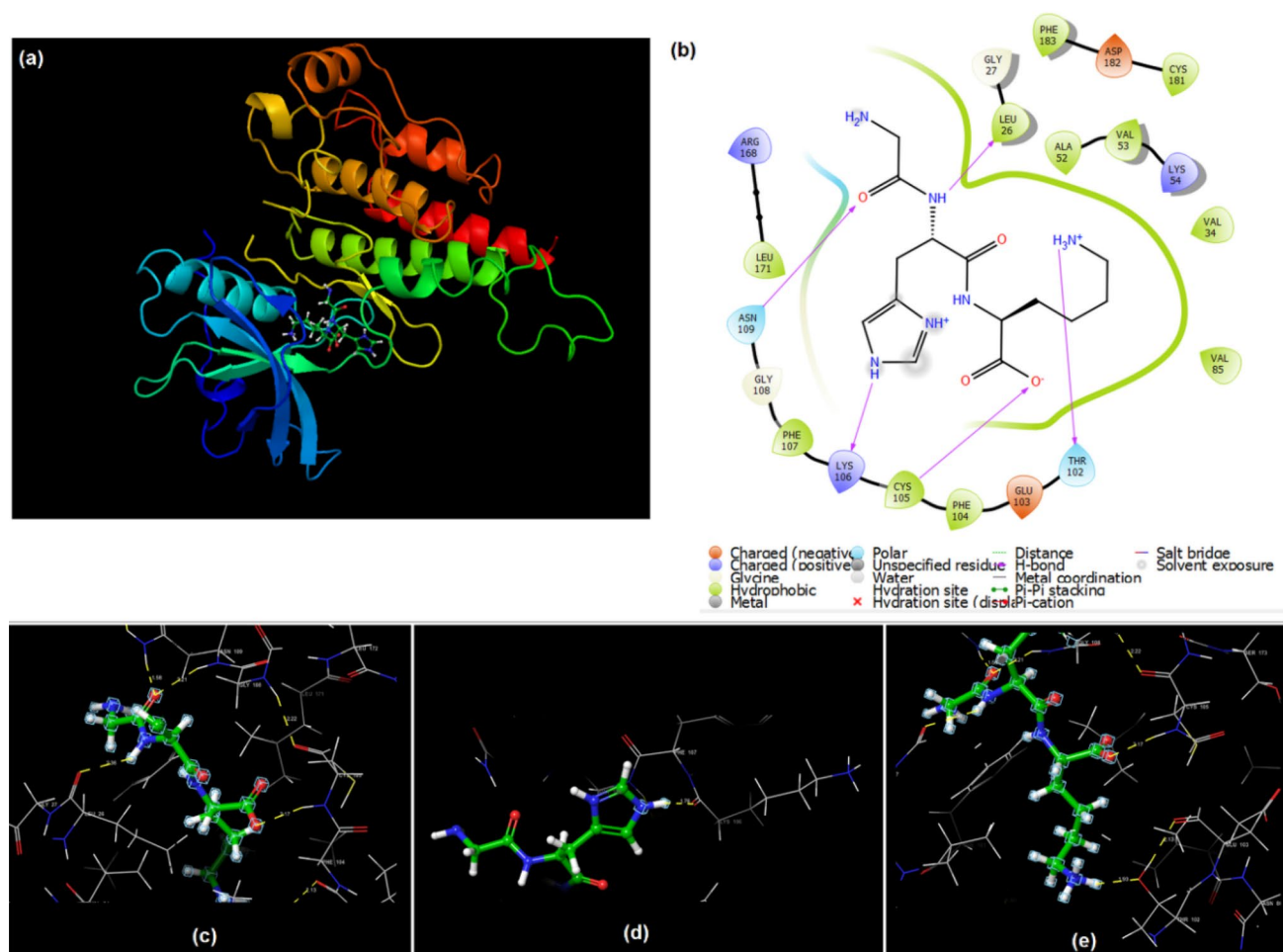
Fig. 5 The docked pose of GHK to VEGFR2 protein (**a**), the 2D ligand interaction of GHK with VEGFR2 protein (**b**). The binding interaction of GHK with amino acid residue ASN-109, LEU-26 and CYS-105 (**c**), LYS-106 (**d**), CYS-105 and THR-102 (**e**)

indicated by the green line, a polar region represented by the blue line, and hydrogen bonds that are effective at stabilizing the binding poses indicated by the purple line were picturized in the 2D ligand interaction graph in Fig. 5b. The GHK docked into the active side was bound with strong hydrogen bonds by the residues ASN-109, LYS-106, CYS-105, THR-102, and LEU-26. The ASN-109 (1.58 Å, 2.21 Å) and LEU-26 (2.36 Å) residues were strongly hydrogen bonded to the backbone of GHK, while the LYS-106 (1.76 Å), CYS-105 (2.17 Å), and THR-102 (1.93 Å) residues respectively made strong hydrogen bonds with the histidine, carboxyl group, and lysine moieties to obtain a stable conformation. The binding interactions of GHK with ASN-109, LYS-106, CYS-105, THR-102, and LEU-26 residues were as shown in Fig. 5c, d, e.

The electrostatic potential map surfaces of the GHK and VEGFR2 protein were also constituted to define the regions that were electron-rich and electron-poor. The lowest potential (electron-rich) regions were expressed in red; while those with the highest potential (electron poor) were shown in blue. Figure 6 also depicts the electrostatic potential map surfaces of ligand and receptors. The oxygen atoms in the carbonyl group with the red region interacted with the blue region with protein (high potential), while the hydrogen atoms in the histidine part tended to incline towards the protein's red region. The pharmacokinetic parameters of drugs such as their permeability towards the blood–brain barrier, skin permeability, percentage oral absorption, and binding to human serum albumin were also calculated and tabulated using the QikProp application of the Maestro software package in Table S4.

In summary, it was determined that the most stable binding poses and binding affinity energies of GHK were obtained as a result of the strong hydrogen bonds in the ASN-109, LYS-106, CYS-105, THR-102, and LEU-26 residues in the active region of the VEGFR2 protein. The pharmacokinetics such as the ADME properties of drug-candidate molecules are also an important point to consider

Fig. 6 The electrostatic potential map surfaces of the VEGFR2 protein and GHK tripeptide
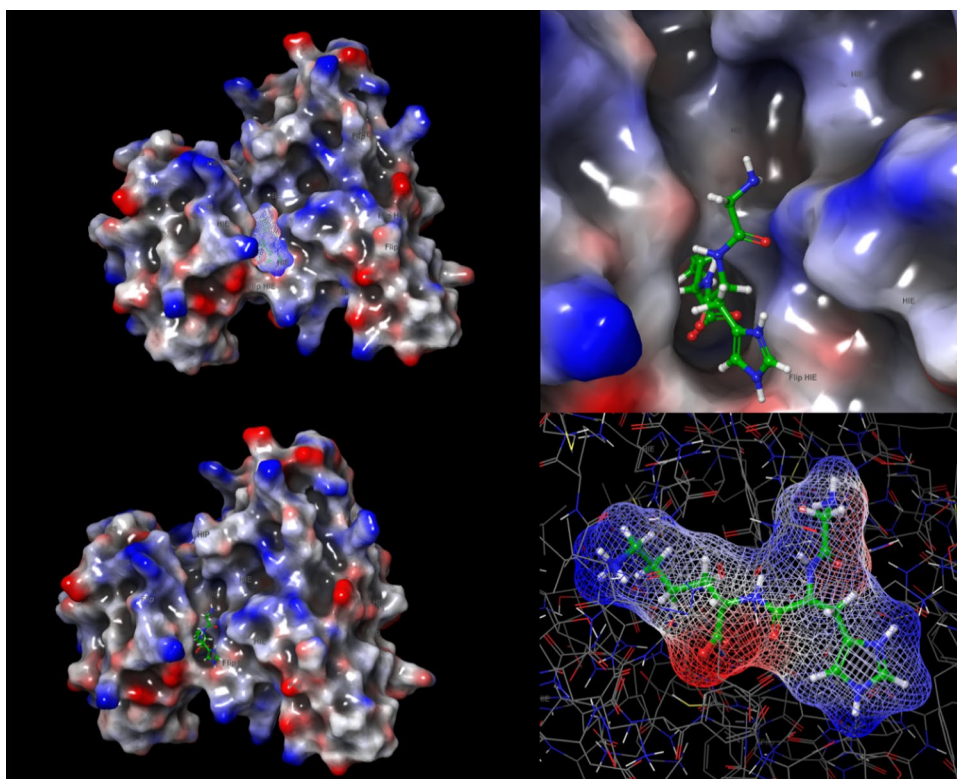
during the drug development process at various points in biological systems. The permeability in the blood–brain barrier, skin permeability, percentage of oral absorption, binding to human serum albumin, and many more useful pharmacokinetic parameters provide substantial information to generate an effective drug in new drug development. The value of QPlogBB for the brain/blood partition coefficient parameter is -2.73, which indicates the drug's ability to pass through the blood–brain barrier. Polymeric nanoparticles are promising drug delivery carriers for the central nervous system due to their encapsulating potential for drugs without excretion and metabolism within the body, and they do not cause any damage when delivered across the blood–brain barrier (Neha et al. 2013). Several in vivo studies have shown that 250 nm and smaller polymeric spherical nanoparticles can cross the blood–brain barrier (Parikh et al. 2010).

FT-IR and Raman Analysis Results

FT-IR, ATR, and Raman spectral analysis were performed to identify probable interactions between the GHK tripeptide and PCL polymer. Figure 7a, b indicate the FT-IR and ATR spectra of blank NPs, free GHK, and GHK-loaded NPs. The different characteristic bands that belong to different functional groups were also assigned and tabulated in Table 1.

The FT-IR spectrum of free GHK observed absorption bands at 1682 cm^{-1}, 1669 cm^{-1}; 1646 cm^{-1}, 1582 cm^{-1};

1515 cm^{-1}, 1325 cm^{-1}, 1307 cm^{-1}, 669 cm^{-1}, 652 cm^{-1} and 572 cm^{-1} corresponding to C=O ester stretching, C=O amide I, C-N–H amid II, C–O–C bending, Ring breathing (His), COOH bending, Ring def. (His), and COOH torsion, respectively. Although, this bands for the encapsulated nanoparticle was observed to be shifted by some amount for GHK-loaded NPs at 1670 cm^{-1}, 1653 cm^{-1}; 1646 cm^{-1}, 1578 cm^{-1}; 1521 cm^{-1}, 1320 cm^{-1}, 1295 cm^{-1}, 710 cm^{-1}, 670 cm^{-1} and 583 cm^{-1}, respectively. Due to the interaction between polymer and GHK tripeptide, C=O amid I stretch vibrations was reduced from 1669 cm^{-1} to 1653 cm^{-1} and C-N–H amid II bending vibrations were shifted from 1515 cm^{-1} to 1521 cm^{-1}. In addition, the carboxyl group stretching and bending and the ring bending, breathing, and deformation of the histidine group were also influenced by this interaction. The same shifts that indicate enhanced hydrogen bonding could also be observed in the ATR and Raman spectra in Table 1.

In addition, the peaks belonging to GHK, which remained under the PCL bands due to encapsulation, were also individually separated using band component analysis. The 1089 cm^{-1}, 1050 cm^{-1} and 1352 cm^{-1} GHK peaks were detected using band component analysis for GHK-loaded PCL in the range 1120 -1000 cm^{-1} and 1440 -1340 cm^{-1} regions for FT-IR-ATR spectra in Fig. S5a-b. For FT-IR, peaks were found at 1307, 1184, 1161, and 1143 cm^{-1} with the aid of the same method by exploring the 1295 cm^{-1}

Fig. 7 The ATR spectrum of GHK, PCL and GHK loaded NPs (**a**), the FT-IR spectrum of GHK, PCL and GHK loaded NPs (**b**)
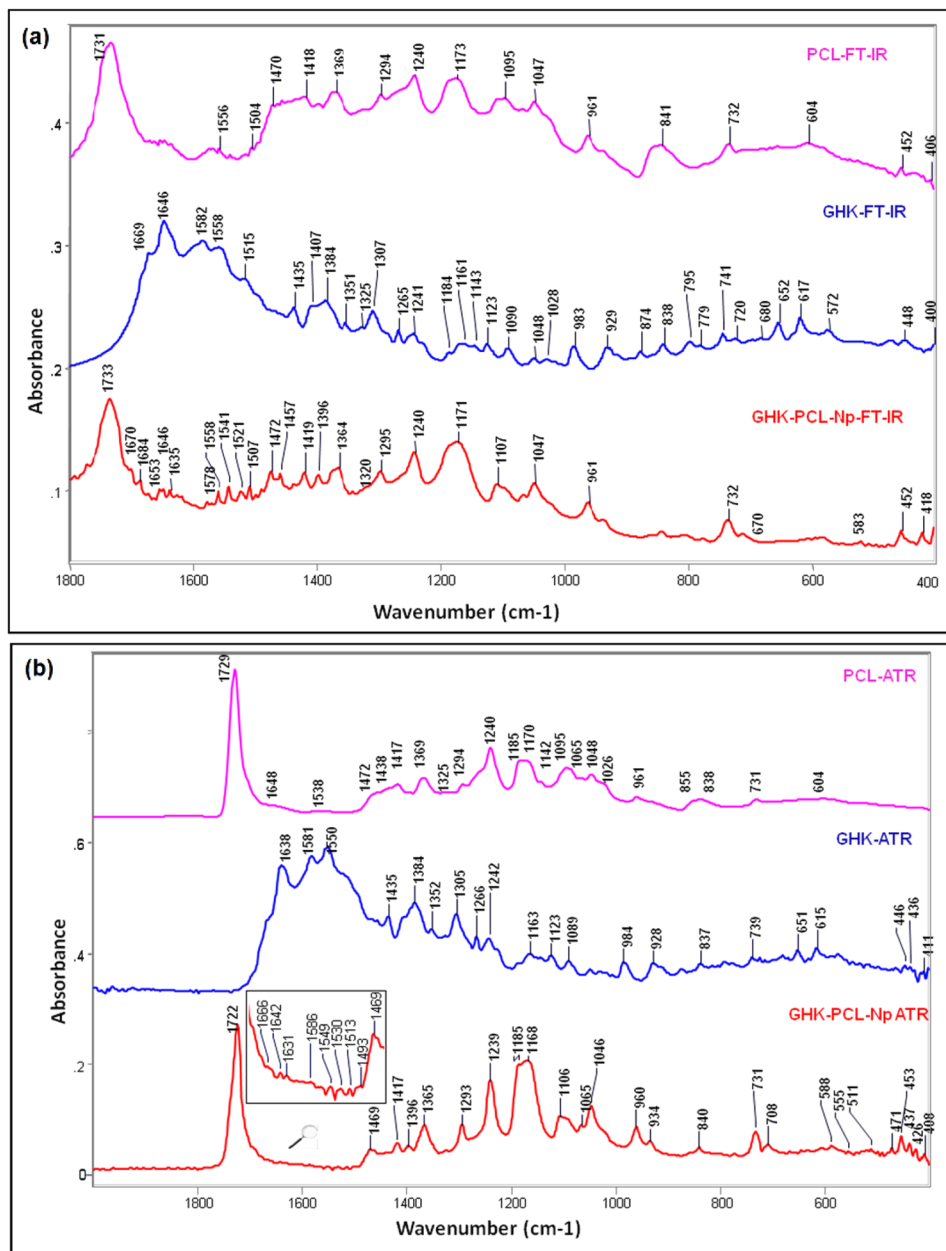
and 1171 cm^{-1} peaks of GHK-loaded-PCL in the range 1120–1130 cm^{-1} and 1284–1320 cm^{-1} in Fig. S6a-b.

In vitro Cytotoxicity of GHK, PCL Nanoparticles, and GHK-Loaded PCL Nanoparticles

Figure 8a shows the cytotoxicity results of GHK, PCL nanoparticles, and GHK-loaded PCL nanoparticles. As seen in the figure, no investigated sample showed toxicity on cells.

The results were similar for different concentrations and the control.

The in vitro Anticancer Effect of GHK

As seen in Fig. 8a, b, GHK has no anticancer or toxic effect on cells in lower concentrations (p > 0,05). However, GHK decreased the viability of glioblastoma cells at higher concentrations while the viability of L929 cells remained the same
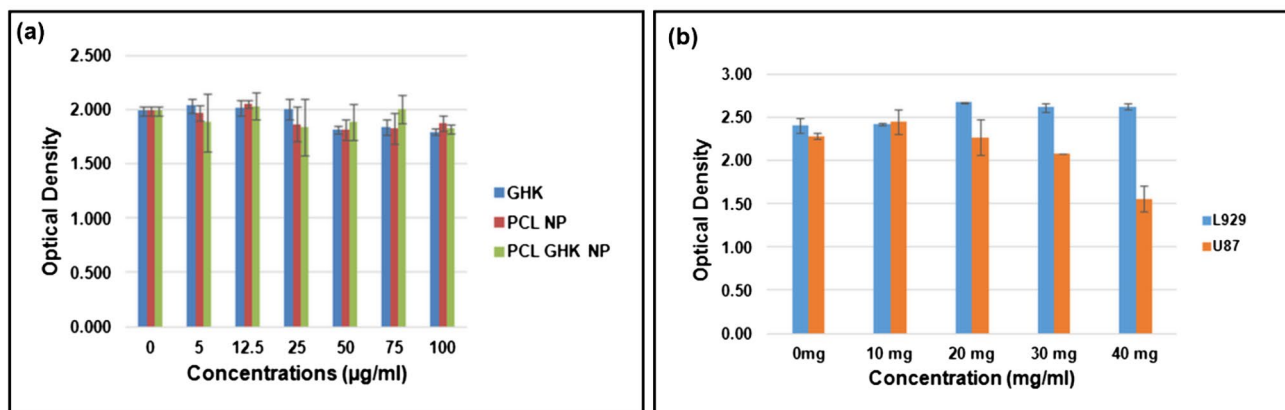
Table 1 The ATR, FT-IR and Raman spectrum of GHK tripeptide and Peptide-loaded PCL NPs particles

Assignment	Glycine (Kumar et al. 2005) Raman	FTIR	Lysine (Amiri et al. 2012) Raman	FTIR	Histidine (Hasegawa et al. 2000) Raman	FTIR	pH 6.8 GHK – GHK Raman	ATR	pH 8.9 GHK (Schirer et al. 2017) – GHK Raman	ATR	GHK (Arul et al. 2005) FTIR	This Study GHK RAMAN Green	RAMAN Red	FTIR	ATR	This Study GHK-PCL NPs Raman	FTIR	ATR
NH	-	3414	3312								3321;3373	3283;3232		3403;3288	3363;3281		3393	-
CH	3050;2930	3084;2920	2975;2936	2789;2654	3130;2987	3127;2984						3026;2953;2915;2858		3074;2952;2932;2859	3003;2952;2933;2905;2878;2857	2914;2873	2944;2867	2943;2865
C=O(ester)	1667	1703	1734	1734							1700;1740	1672		1682	1682	1729;1665	1733;1670	1722;1666
C=O(amidI)								1657		1648	1622;1648	1650	-	1669;1646	1638	1631	1653;1646	1631
CNH(amidII)							1585	1563	1585	1585	1551;1536;1515	1575;1572;1514	1581;1569;1510	1582;1540;1515	1581;1550	1588;1567;1512	1578;1541;1521	1586;1568;1549
HNH bending	-	1610	-	1619										1577	1566			
C=C(His)					1573	1575	1568		1569			1552	1555	1558	1557		1558	
HCH sci	1410	1410	1445	1445	1490	1490						1448;1444	1464;1446;1442	1465;1456;1435	1470;1456;1435	1477;1445;1426	1472;1457;1437	1469;1462;1417
C=N(His)					1424	1423							1386;	1407;1384	1406;1384	1388	1396	1396
NH2twist + CH2twist	1323	1334	1352	1355								1342		1351	1352	1355	1364	1365
C-O and C-O-C			-	1331								1342	1337;1154	1325;1143	1326;1144	1332;1144	1320	1327
Ring breathing (His)					1301	1304	1267		1267			1310	1305	1307	1305	1307	1295	1293
C-N(His)					1085	1087	-	1104;1086	-	1105;1084		1102;1090	1093	1115;1090	1123;1089	1114;1099	1107;1095	1106;1092
Ring bending(His)					975;935	975;941						988	985;932	983;929	984;928	992;921	961;934	960;934
COOH bending			-									688	680	669	669	667	710	708
Ring def. (His)					660	664						651	653	652	651	656	670	667
COOH torsion												570;521	570;529	572;543	575;546	572;549	583;547	588;540

Fig. 8 In vitro cytotoxicity of GHK tripeptide, PCL nanoparticles, and GHK-loaded PCL nanoparticles (**a**), In vitro anticancer effect of GHK on U87 cells

as the control. Particularly at the 40 mg/mL concentration, the cell viability decreased to nearly 65%.

Conclusion

GHK is a tripeptide with multiple biological activities such as antioxidant, wound healing, anti-inflammation, anti-pain and anti-anxiety effects; it has also been proposed as a therapeutic peptide for cancer. Some in vitro studies have been conducted on the anticancer effect of GHK on prostate, breast cancer and human nerve cancer. In this study, the effect of GHK tripeptide and its nano-sized formulation on glioblastoma cells was investigated for the first time.

In our study, optimized GHK-loaded PCL nanoparticles were obtained with 232.5 ± 0.72 average particle size and -10.8 ± 0.64 mV zeta potential. The usage potential of GHK nanoformulation for cancer threapy was investigated via in silico and in vitro methods. It is believed that the GHK-loaded PCL nanoparticles may demonstrate the potential to cross the blood barrier, and can be used as a therapeutic agent, particularly in the area of nervous diseases.

Author Contribution YBK: Supervision, Data curation, Conceptualization, Writing- Reviewing and Editing. SKG: Supervision, Data curation, Conceptualization, Writing- Reviewing and Editing. RCK: Data Curation, Writing. BA: Data curation. BB: Data curation, Writing- Reviewing and Editing. YK: Data curation. AEO: Writing, Reviewing. SA: Writing, Reviewing.

Declarations

References

Abamor EŞ (2018) A New Approach to the Treatment of Leıshmaniasis: Quercetin-Loaded Polycaprolactone Nanoparticles. J Turkish Chem Soc Sect Chem 5:1071–1082

Abascal JL, Vega C (2005) A general purpose model for the condensed phases of water: TIP4P/2005. J Chem Phys 123:234505

Amiri A, Zardini HZ, Shanbedi M, Maghrebi M, Baniadam M, Tol-ueinia B (2012) Efficient method for functionalization of carbon nanotubes by lysine and improved antimicrobial activity and water-dispersion. Mater Lett 72:153–156

Arul V, Gopinath D, Gomathi K, Jayakumar R (2005) Biotinylated GHK peptide incorporated collagenous matrix: A novel biomaterial for dermal wound healing in rats Journal of Biomedical Materials Research Part B: Applied Biomaterials: An Official Journal of The Society for Biomaterials. The Japanese Society for Biomaterials, and the Australian Society for Biomaterials and the Korean Society for Biomaterials 73:383–391

Bienert S, Waterhouse A, de Beer TA, Tauriello G, Studer G, Bordoli L, Schwede T (2017) The SWISS-MODEL Repository—new features and functionality. Nucleic Acids Res 45:D313–D319

Bilensoy E, Sarisozen C, Esendağlı G, Doğan AL, Aktaş Y, Şen M, Mungan NA (2009) Intravesical cationic nanoparticles of chitosan and polycaprolactone for the delivery of Mitomycin C to bladder tumors. Int J Pharm 371:170–176

Brannon-Peppas L, Blanchette JO (2004) Nanoparticle and targeted systems for cancer therapy. Adv Drug Deliv Rev 56:1649–1659

Brigger I, Dubernet C, Couvreur P (2012) Nanoparticles in cancer therapy and diagnosis. Adv Drug Deliv Rev 64:24–36

Budama-Kilinc Y, Ozdemir B, Gozutok K (2017) Peptide-based nano-biomaterials. In: Razavi M, Thakor A (eds) Nanobiomaterials Science, Development and Evaluation. Elsevier, Amsterdam, pp 135–146

Bussi G, Donadio D, Parrinello M (2007) Canonical sampling through velocity rescaling. J Chem Phys 126:014101

Çalman F, Arayıcı PP, Büyükbayraktar HK, Karahan M, Mustafaeva Z, Katsarava R (2019) Development of vaccine prototype against Zika virus disease of peptide-loaded PLGA nanoparticles and evaluation of cytotoxicity. Int J Pept Res Ther 25:1057–1063

Case D et al (2018) AMBER 2018. Univ California, San Fr

Chawla JS, Amiji MM (2002) Biodegradable poly (ε-caprolactone) nanoparticles for tumor-targeted delivery of tamoxifen. Int J Pharm 249:127–138

Choi HR, Kang YA, Ryoo SJ, Shin JW, Na JI, Huh CH, Park KC (2012) Stem cell recovering effect of copper-free GHK in skin. J Pept Sci 18:685–690

Da Silva AWS, Vranken WF (2012) ACPYPE-Antechamber Python Parser Interface. BMC Res Notes 5:1–8

Friesner RA et al (2004) Glide: a new approach for rapid, accurate docking and scoring. 1 Method and Assessment of Docking Accuracy. J Med Chem 47:1739–1749

Frisch M et al (2009) Gaussian 09, Revision D. 01, 2009. Gaussian Inc, Wallingford CT

Frisch M et al (2016) Gaussian 16. Gaussian, Inc., Wallingford, CT

Govender T, Stolnik S, Garnett MC, Illum L, Davis SS (1999) PLGA nanoparticles prepared by nanoprecipitation: drug loading and release studies of a water soluble drug. J Control Release 57:171–185

Guo J et al (2011) Aptamer-functionalized PEG–PLGA nanoparticles for enhanced anti-glioma drug delivery. Biomaterials 32:8010–8020

Halgren TA, Murphy RB, Friesner RA, Beard HS, Frye LL, Pollard WT, Banks JL (2004) Glide: a new approach for rapid, accurate docking and scoring. 2 Enrichment Factors in Database Screening. J Med Chem 47:1750–1759

Harder E et al (2016) OPLS3: a force field providing broad coverage of drug-like small molecules and proteins. J Chem Theory Comput 12:281–296

Hasegawa K, Ono T-a, Noguchi T (2000) Vibrational spectra and ab initio DFT calculations of 4-methylimidazole and its different protonation forms: infrared and Raman markers of the protonation state of a histidine side chain. J Phys Chem B 104:4253–4265

Hicklin DJ, Ellis LM (2005) Role of the Vascular Endothelial Growth Factor Pathway in Tumor Growth and Angiogenesis. J Clin Oncol 23:1011–1027

Hornak V, Abel R, Okur A, Strockbine B, Roitberg A, Simmerling C (2006) Comparison of multiple Amber force fields and development of improved protein backbone parameters Proteins: Structure. Function, and Bioinformatics 65:712–725

Humphrey W, Dalke A, Schulten K (1996) VMD: visual molecular dynamics. J Mol Graph 14:33–38

Kang Y-A et al (2009) Copper–GHK increases integrin expression and p63 positivity by keratinocytes. Arch Dermatol Res 301:301–306

Karahan M (2021) Synthetic Peptide Vaccine Models: Design, Synthesis, Purification and Characterization. CRC Press, Boca Raton

Kokcu Y et al (2020) Structural analysis, molecular dynamics and docking calculations of skin protective tripeptide and design, characterization, cytotoxicity studies of its PLGA nanoparticles. J Mol Struct 1200:127046

Kolluru LP, Chandran T, Shastri PN, Rizvi SA, D'Souza MJ (2020) Development and evaluation of polycaprolactone based docetaxel nanoparticle formulation for targeted breast cancer therapy. J Nanopart Res 22:1–14

Kumar SS (2019) Formulation and characterization of noscapine-loaded polycaprolactone nanoparticles Asian Journal of Pharmaceutics (AJP): Free full text articles from Asian. J Pharm. https://doi.org/10.22377/ajp.v13i01.3003

Kumar S, Rai AK, Singh V, Rai S (2005) Vibrational spectrum of glycine molecule. Spectrochim Acta Part A Mol Biomol Spectrosc 61:2741–2746

Lamprecht A, Ubrich N, Pérez MH, Lehr C-M, Hoffman M, Maincent P (2000) Influences of process parameters on nanoparticle preparation performed by a double emulsion pressure homogenization technique. Int J Pharm 196:177–182

Lipinski C, Lombardo F, Dominy B, Feeney P (1997) Toward minimalistic modeling of oral drug absorption. Adv Drug Deliv Rev 23:3–25

Lokhande A, Mishra S, Kulkarni R, Naik J (2015) Development and Evaluation of Nateglinide Loaded Polycaprolactone Nanoparticles. Micro Nanosyst 7:43–48

Neha B, Ganesh B, Preeti K (2013) Drug Delivery to the Brain Using Polymeric Nanoparticles: a Review International. J Pharm Life Sci 2:107–132

Öztürk K, Mashal AR, Yegin BA, Çalış S (2017) Preparation and in vitro evaluation of 5-fluorouracil-loaded PCL nanoparticles for colon cancer treatment. Pharmaceutical Dev Technol 22:635–641

Parikh T, Bommana MM, Squillante E (2010) Efficacy of Surface Charge in Targeting Pegylated Nanoparticles of Sulpiride to the Brain European. J Pharm Biopharm 74:442–450

Park S-I, Heo SH, Lee J, Cha H, Shin MS (2021) A Clinical Study on Anti-Wrinkle Efficacy of a Cosmetics Containing Oligoarginine Conjugation of Palmitoyl-GHK Peptide for Skin Penetrating. Turkish Journal of Computer and Mathematics Education (TURCOMAT) 12:401–406

Parrinello M, Rahman A (1981) Polymorphic Transitions in Single Crystals: A New Molecular Dynamics Method. J Appl Phys 52:7182–7190

Paulo CS, Neves RP, Ferreira LS (2011) Nanoparticles for intracellular-targeted drug delivery. Nanotechnology 22:494002

Peer D, Karp JM, Hong S, Farokhzad OC, Margalit R, Langer R (2007) Nanocarriers as an emerging platform for cancer therapy. Nat Nanotechnol 2:751–760

Pickart L (2008) The human tri-peptide GHK and tissue remodeling Journal of Biomaterials Science. Polymer Edition 19:969–988

Pickart L (2009) The human tripeptide GHK (Glycyl-l-Histidyl-l-Lysine) T he copper switch, and the treatment of degenerative conditions of aging. Anti-Aging Therapeutics 11:301–312

Pickart L, Margolina A (2012) Anti-Aging Activity of the GHK Peptide-the Skin and beyond. J Aging Res Clin Pract 1:13–15

Pickart L, Freedman JH, Loker WJ, Peisach J, Perkins CM, Stenkamp RE, Weinstein B (1980) Growth-modulating plasma tripeptide may function by facilitating copper uptake into cells. Nature 288:715–717

Pickart L, Vasquez-Soltero JM, Margolina A (2012) The human tripeptide GHK-Cu in prevention of oxidative stress and degenerative conditions of aging: implications for cognitive health. Oxid Med Cell Longev. https://doi.org/10.1155/2012/324832

Pickart L, Vasquez-Soltero JM, Margolina A (2017) The Effect of the Human Peptide GHK on Gene Expression Relevant to Nervous System Function and Cognitive Decline. Brain Sci 7:20

Potashman MH et al (2007) Design, synthesis, and evaluation of orally active benzimidazoles and benzoxazoles as vascular endothelial growth factor-2 receptor tyrosine kinase inhibitors. J Med Chem 50:4351–4373

Sastry GM, Adzhigirey M, Day T, Annabhimoju R, Sherman W (2013) Protein and ligand preparation: parameters, protocols, and influence on virtual screening enrichments. J Comput Aided Mol Des 27:221–234

Schirer A, El Khoury Y, Faller P, Hellwig P (2017) Similarities and differences of copper and zinc cations binding to biologically relevant peptides studied by vibrational spectroscopies JBIC. J Biol Inorg Chem 22:581–589

Shuai X, Ai H, Nasongkla N, Kim S, Gao J (2004) Micellar carriers based on block copolymers of poly (ε-caprolactone) and poly (ethylene glycol) for doxorubicin delivery. J Control Release 98:415–426

Søndergaard CR, Olsson MH, Rostkowski M, Jensen JH (2011) Improved treatment of ligands and coupling effects in empirical calculation and rationalization of p K a values. J Chem Theory Comput 7:2284–2295

Taylor RD, Jewsbury PJ, Essex JW (2002) A review of protein-small molecule docking methods. J Comput Aided Mol Des 16:151–166

Tinca AL, Iurian S, Rus LM, Porfire A, Tefas LR (2020) Development and characterization of curcumin-loaded polycaprolactone nanoparticles by Design of Experiments. Ro J Pharm Pract. https://doi.org/10.37897/RJPhP.2020.3.3

Türkoğlu M, Erdem S (2010) Glycyl-l-histidyl-l-liysine-Cu (2+) loaded liposome formulations. MARMARA Pharm J. https://doi.org/10.12991/201014455

Turner P (2005) XMGRACE, Version 5.1. 19 Center for Coastal and Land-Margin Research. Oregon Graduate Institute of Science and Technology, Beaverton, OR

Van Der Spoel D, Lindahl E, Hess B, Groenhof G, Mark AE, Berendsen HJ (2005) GROMACS: fast, flexible, and free. J Comput Chem 26:1701–1718

Yang Y-Y, Chung T-S, Ng NP (2001) Morphology, drug distribution, and in vitro release profiles of biodegradable polymeric microspheres containing protein fabricated by double-emulsion solvent extraction/evaporation method. Biomaterials 22:231–241

Yuriev E, Agostino M, Ramsland PA (2011) Challenges and advances in computational docking: 2009 in review. J Mol Recognit 24:149–164